


 Cite this: *Phys. Chem. Chem. Phys.*,
 2023, 25, 6473

Substitution of Ca²⁺ and changes in the H-bond network near the oxygen-evolving complex of photosystem II†

 Manoj Mandal, *^a Keisuke Saito ^{bc} and Hiroshi Ishikita *^{bc}

Ca²⁺, which provides binding sites for ligand water molecules W3 and W4 in the Mn₄CaO₅ cluster, is a prerequisite for O₂ evolution in photosystem II (PSII). We report structural changes in the H-bond network and the catalytic cluster itself upon the replacement of Ca²⁺ with other alkaline earth metals, using a quantum mechanical/molecular mechanical approach. The small radius of Mg²⁺ makes W3 donate an H-bond to D1-Glu189 in Mg²⁺-PSII. If an additional water molecule binds at the large surface of Ba²⁺, it donates H-bonds to D1-Glu189 and the ligand water molecule at the dangling Mn, altering the H-bond network. The potential energy profiles of the H-bond between D1-Tyr161 (TyrZ) and D1-His190 and the interconversion between the open- and closed-cubane S₂ conformations remain substantially unaltered upon the replacement of Ca²⁺. Remarkably, the O5...Ca²⁺ distance is shortest among all O5...metal distances irrespective of the radius being larger than that of Mg²⁺. Furthermore, Ca²⁺ is the only alkaline earth metal that equalizes the O5...metal and O2...metal distances and facilitates the formation of the symmetric cubane structure.

 Received 27th October 2022,
 Accepted 6th February 2023

DOI: 10.1039/d2cp05036f

rsc.li/pccp

The reaction center of the water-splitting enzyme photosystem II (PSII) is formed by two structurally similar but electrostatically different protein subunits, D1 and D2.^{1,2} To oxidize substrate water molecules, PSII uses the electron transfer pathway that proceeds from the catalytic Mn₄CaO₅ cluster *via* redox active D1-Tyr161 (TyrZ) to the oxidized chlorophyll pair, [P_{D1}P_{D2}]^{•+} (≈ P_{D1}^{•+}+³⁻⁶). [P_{D1}P_{D2}]^{•+} forms after electronic excitation of the reaction center chlorophylls^{7,8} and subsequent electron transfer occurs *via* pheophytin and the initial quinone Q_A to the secondary quinone Q_B. As electron transfer occurs, the oxidation state of the oxygen-evolving complex, S_n, increases from S₀ to S₃ in the order S₀ → S₁ → S₂ → S₃ → S₀ (*e.g.*,^{9,10}). O₂ evolves during the S₃ to S₀ transition after S₃ absorbs a photon.

The Mn₄CaO₅ cluster has four water molecules as ligands, W1 and W2 at the dangling Mn (Mn4) and W3 and W4 at Ca²⁺, which are also candidates for substrate water molecules (*e.g.*,^{11,12}). Ca²⁺ has seven ligand groups (O1, O2, O5, D1-

Asp170, D1-Ala344, W3, and W4).¹ Ca²⁺ and Mg²⁺ are the most abundant alkaline earth metals in biological systems. In PSII, Ca²⁺ is a prerequisite for O₂ evolution.¹³⁻¹⁹ Previously, it was speculated that Ca²⁺ was the origin of the distorted cubane structure (*e.g.*,²⁰). However, the distortion of the Mn₄CaO₅ cluster remains even upon the removal of Ca²⁺.²¹⁻²³ Indeed, not Ca²⁺ but dangling Mn4 is most responsible for the distortion of the cluster shape.²³ The S₂ to S₃ transition is inhibited in Ca²⁺-depleted PSII.^{13,24-26} Ca²⁺ depletion not only causes the alteration of the H-bond network at the Mn₄O₅ and TyrZ moieties²³ but also decreases the redox potential (*E*_m) of TyrZ significantly due to reorientation of the water molecules in the H-bond network, making electron transfer from the Mn₄CaO₅ cluster to TyrZ uphill.²⁷

Replacement of Ca²⁺ with any metals except Sr²⁺ inhibits O₂ evolution,¹³⁻¹⁷ although the inhibition mechanism may depend on the metals. The geometry of the catalytic site in Sr²⁺-substituted PSII (Sr²⁺-PSII) resembles that of native PSII (Ca²⁺-PSII).^{28,29} The *E*_m values for the artificial clusters with Sr²⁺ are also similar to those with Ca²⁺.³⁰⁻³² The *E*_m value for the Mn₄BaO₅ cluster in Ba²⁺-substituted PSII (Ba²⁺-PSII) is also considered to be similar to that for the Mn₄CaO₅ cluster in native PSII based on the observation of the normal thermoluminescence S₂Q_A^{•-} band.³³ Fourier transform infrared (FTIR) studies by Kimura *et al.* showed that the double difference S₂/S₁ spectrum was not affected significantly upon the substitution of Ca²⁺ with Mg²⁺ and Sr²⁺, whereas the vibrational modes of the

^a Department of Chemical and Biological Sciences, S. N. Bose National Centre for Basic Sciences, Kolkata 700106, West Bengal, India.

E-mail: mandalmanojcu@gmail.com

^b Research Center for Advanced Science and Technology, The University of Tokyo, 4-6-1 Komaba, Meguro-ku, Tokyo 153-8904, Japan.

E-mail: hiro@appchem.t.u-tokyo.ac.jp

^c Department of Applied Chemistry, The University of Tokyo, 7-3-1 Hongo, Bunkyo-ku, Tokyo 113-8654, Japan

 † Electronic supplementary information (ESI) available. See DOI: <https://doi.org/10.1039/d2cp05036f>


carboxylate ligand residue disappeared upon substitution with Ba^{2+} in the PSII membrane from spinach.³³ According to FTIR studies by Suzuki *et al.*,³⁴ more than three carboxylate residues, except D1-Glu189 and the carboxyl terminus of the D1 protein, D1-Ala344, were perturbed upon Sr^{2+} substitution. FTIR studies by Strickler *et al.* also suggested that D1-Ala344 was not involved in the perturbation observed upon Sr^{2+} substitution.³⁵

S_2 can form in Mg^{2+} -substituted PSII (Mg^{2+} -PSII) but not in Ba^{2+} -PSII.³⁶ Vrettos *et al.* reported that Mg^{2+} and Ba^{2+} are unlikely to bind competitively with Ca^{2+} .¹⁴ It was proposed that Ba^{2+} led to the deformation of the proton-conducting H-bond network.^{37,38} Although the radius of Ca^{2+} is one of the key factors,^{14,32} it remains unclear what property of Ca^{2+} is specifically required for O_2 -evolving activity among alkaline earth metals. Previous theoretical studies by Vogt *et al.* showed the detailed geometry of the Mn_4SrO_5 cluster in S_1 , S_0 , S_{-1} , and S_{-2} in Sr^{2+} -PSII.²⁹ On the other hand, not only the geometry of the Mn_4SrO_5 cluster but also the energetics of the H-bond network in S_2 , in which the significance of Ca^{2+} is pronounced, remains unclear. FTIR studies suggested that the S_2 to S_3 transition involves the migration of the proton of a ligand water molecule toward D1-Asp61,³⁹ which is in line with mutational studies (mutated to the other 19 residues).⁴⁰ Theoretical studies also showed that a low-barrier H-bond forms between the ligand water molecule W1 and D1-Asp61 specifically in S_2 .^{41,42} The replacement of Ca^{2+} with the other redox-inactive divalent metals is unlikely to affect the H-bond between W1 and D1-Asp61, as the Ca^{2+} binding site is not directly involved in the $\text{W1} \cdots \text{D1-Asp61}$ moiety. In contrast, the redox-active TyrZ \cdots D1-His190 pair is directly involved in the H-bond network of the Ca^{2+} binding site.²³ Because TyrZ forms a low-barrier H-bond with D1-His190⁴³ and is directly involved in the H-bond network of the ligand water molecules (W3 and W4) at Ca^{2+} ,^{23,27} Ca^{2+} -substitution may affect the low-barrier H-bond formation between TyrZ and D1-His190. However, to the best of our knowledge, the influence of Ca^{2+} on the TyrZ \cdots D1-His190 H-bond has not been specifically reported.

To understand the specificity of Ca^{2+} in PSII, we investigated the local geometry of the metal-substituted Mn_4MO_5 cluster ($\text{M} = \text{Mg}^{2+}$, Sr^{2+} , and Ba^{2+}) in S_2 with Mn1(III)Mn2(IV)Mn3(IV)Mn4(IV) (open-cubane S_2 conformation) by adopting a quantum mechanical/molecular mechanical (QM/MM) approach based on the native Ca^{2+} -PSII crystal structure. As proton transfer occurs most effectively in the well-ordered H-bond network^{44,45} and the water molecules in the focusing H-bond network are less disordered in molecular dynamics simulations,⁴⁶ comparisons of the H-bond networks among the metal-substituted PSIIIs based on the QM/MM-optimized geometries are, therefore, the best starting point.

Methods

Coordinates and atomic partial charges

The atomic coordinates were obtained from the X-ray structure of PSII from *Thermosynechococcus vulcanus* (PDB code, 3ARC).¹

The positions of all heavy atoms were fixed during the optimization of the positions of H atoms with CHARMM.⁴⁷ All titratable groups (*e.g.*, acidic and basic groups) were ionized. D1-His337 was considered to be protonated.⁴⁸ Atomic partial charges of the amino acids and cofactors were obtained from the CHARMM22⁴⁹ parameter set and previous studies,⁴⁵ respectively.

QM/MM calculations

The unrestricted density functional theory method was employed with the B3LYP functional (commonly used for PSII by, *e.g.*, Amin,⁵⁰ Batista,⁵¹ Guidoni,⁵² Ishikita,⁴⁵ Pace,⁵³ Siegbahn,⁵⁴ Yamaguchi,⁵⁵ and their coworkers as summarized in ref. 56) and LACVP* basis sets (LANL2DZ (double ζ quality basis set with the Los Alamos effective core potential) for Mn, Mg, Ca, Sr, and Ba atoms and 6-31G* for other atoms)⁵⁷ using the QSite⁵⁸ program if not otherwise specified. The M06 functional was also used to evaluate the contributions of dispersion correction. See Table S1 (ESI[†]) for the results obtained with other functional/basis sets. All water molecules assigned in the crystal structure were included in the present study. FTIR spectra and theoretical calculations by Nakamura and Noguchi suggested that the ligand water molecules, W1 and W2, are H_2O in S_1 and S_2 .⁴⁸ pK_a calculations by Saito *et al.* showed that W1 and W2, were H_2O and $\text{pK}_a(\text{W2})$ was only marginally (~ 1 pK_a unit) lower than $\text{pK}_a(\text{W1})$ in water, whereas $\text{pK}_a(\text{W1})$ was significantly lower than $\text{pK}_a(\text{W2})$ in the PSII protein environment due to the presence of the proton acceptor, D1-Asp61.⁴² In the open-cubane S_2 conformation, H_2O at W2 forms a low-barrier H-bond with D1-Asp61, although the proton remains at this moiety.⁴¹ In the present study, W1 and W2 were modeled as H_2O . Counter ions were added to neutralize the entire system. In the QM region, all atomic coordinates were fully relaxed (*i.e.*, not fixed at the positions in the crystal structure). For the MM region, the atomic charges of CHARMM22 were used for amino acid groups to facilitate comparison between their influences on the active site in the QM region and their influences on E_m for further purposes, as E_m can be calculated using the atomic charges of CHARMM22 and solving the Poisson–Boltzmann equation (*e.g.*,⁵⁹). In the MM region, only the H atom positions were optimized using the OPLS2005 force field, which is mandatory in QSite. In the MM region, the heavy atom positions were fixed to avoid unexpected conformational changes (*e.g.*, caused by the absence of water molecules unassigned in the original crystal structure). In QSite, the QM and MM regions interact *via* electrostatic and van der Waals interactions.

The Mn_4CaO_5 cluster was considered to be in the S_2 states with antiferromagnetically coupled Mn ions; the resulting Mn oxidation states (Mn1, Mn2, Mn3, Mn4) and the total spin, S , were (III, IV, IV, IV) and $S = 7/2$ ($\uparrow \downarrow \uparrow \uparrow$) in S_2 , respectively. It should be noted that the difference in S (*e.g.*, $S = 1/2$ in S_2 ,⁶⁰ high, low, ferromagnetic, and antiferromagnetic) did not affect the values; for example, (i) the resulting geometry^{61,62} and (ii) the potential-energy profile of proton transfer⁴¹ are not crucial



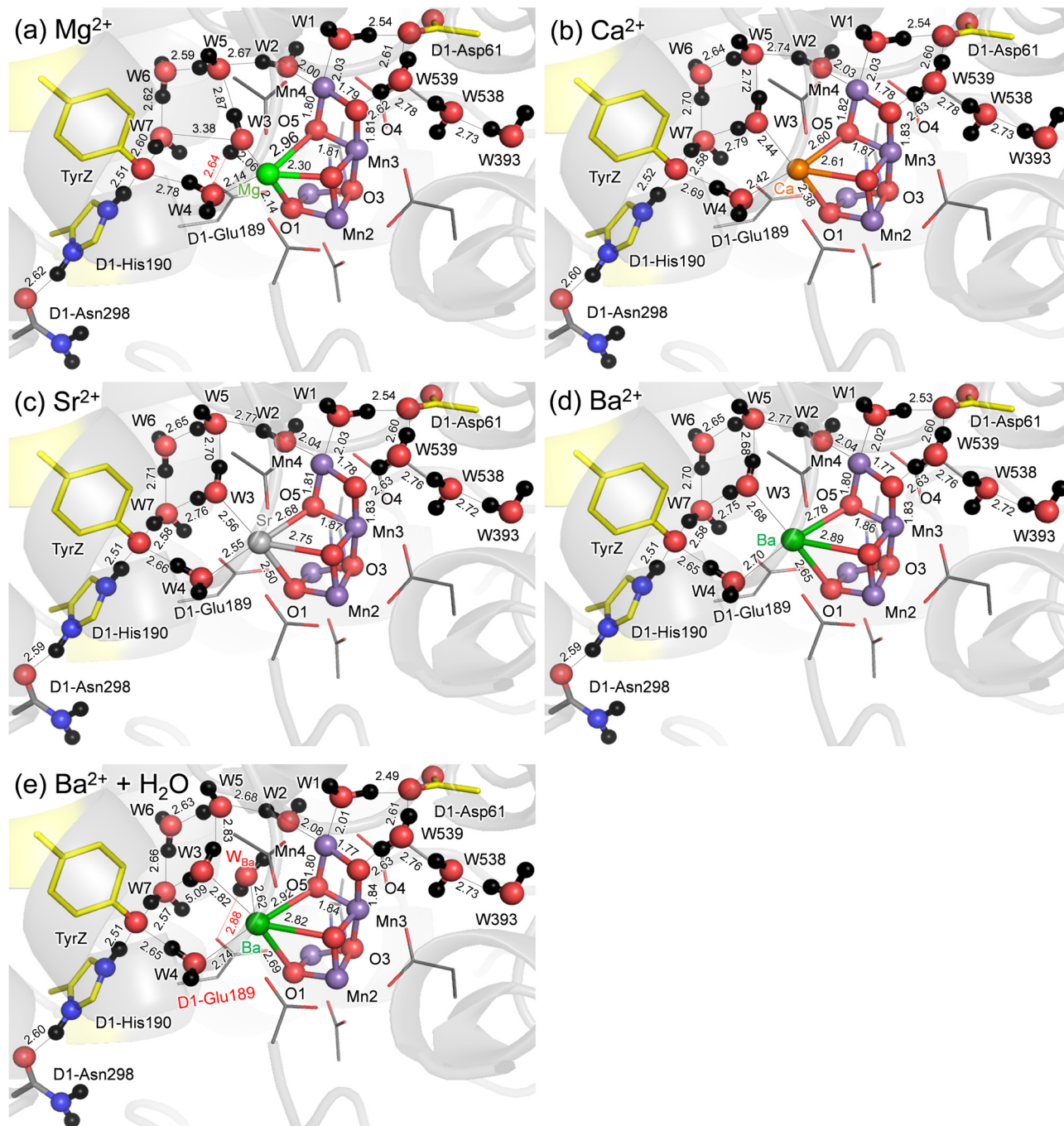


Fig. 1 QM/MM-optimized geometries in the open-cubane S_2 conformations. (a) Mg^{2+} -PSII. (b) Ca^{2+} -PSII. (c) Sr^{2+} -PSII. (d) Ba^{2+} -PSII. (e) Ba^{2+} -PSII with an additional water molecule at Ba^{2+} (W_{Ba}). Dotted lines indicate H-bonds. Bond distances are in Å.

to the spin configurations as far as the protein electrostatic environment is fully included.⁶³

The initial-guess wavefunctions were obtained using ligand field theory⁶⁴ implemented in the QSite program. For native PSII, the QM region was defined as the Mn_4MO_5 cluster (including the ligand side-chains of D1-Asp170, D1-Glu189, D1-His332, D1-Glu333, D1-Asp342, and CP43-Glu354; ligand carboxy-terminal group of D1-Ala344; and ligand water molecules, W1–W4), O4–water chain (W539, W538, and W393),^{45,65}

Cl-1 binding site (Cl^- , W442, W446, and the side-chains of D1-Asn181 and D2-Lys317), second-sphere ligands (side-chains of D1-Asp61 and CP43-Arg357), H-bond network of TyrZ (side-chains of D1-Tyr161, D1-His190, and D1-Asn298), including the diamond-shaped water cluster (W5, W6, and W7).^{43,66} The QM region defined in the present study is one of the largest among theoretical studies of PSII, which essentially covers the entire H-bond network of the ligand water molecules at the Ca^{2+} moiety (summarized in ref. 56).



Table 1 Distances of the open-cubane Mn_4MO_5 clusters in S_2 ($M = Mg^{2+}$, Ca^{2+} , Sr^{2+} , and Ba^{2+}) in Å

	Mg^{2+}	Ca^{2+}	Sr^{2+}	Ba^{2+}	$Ba^{2+} + \text{water}$
Ionic radius ^a	0.66	0.99	1.12	1.34	1.34
(Surface area ratio ^b)	(0.44)	(1)	(1.28)	(1.83)	(1.83)
W3···M	2.06	2.44	2.56	2.68	2.82
W4···M	2.14	2.42	2.55	2.70	2.74
O1···M	2.14	2.38	2.50	2.65	2.69
O2···M	2.30	2.61	2.75	2.89	2.82
O5···M	2.96	2.60	2.68	2.78	2.92
O5···Mn1	2.93	3.08	3.08	3.12	3.15
O5···Mn4	1.80	1.82	1.81	1.80	1.80

^a See ref. 67. ^b The surface area of Ca^{2+} is normalized to 1.

To obtain the potential energy profiles of the $O\cdots H^+\cdots N$ bond for TyrZ···D1-His190, the QM/MM-optimized geometry was used as the initial geometry. The H atom under investigation was moved between the O and N moieties by 0.05 Å, after which the geometry was optimized by constraining the distance between $O-H^+$ and H^+-N , and the energy was calculated. This procedure was repeated until the H atom reached the O moieties. To obtain the potential energy profiles of the Mn1···O5 and O5···Mn4 bonds for the open- and closed-cubane S_2 conformations, the QM/MM-optimized geometry of the open-cubane S_2 conformation was used as the initial geometry. The O5 was moved toward the Mn4 moiety by 0.05 Å, after which the geometry was optimized by constraining the Mn1···O5 distance, and the energy was calculated.

Results

H-bond network

QM/MM calculations show that the difference in the geometry is predominantly observed at the **M** binding moiety of the Mn_4MO_5 cluster (Fig. 1). Among the three metal-substituted PSII, Sr^{2+} -PSII is closest to Ca^{2+} -PSII, as the H-bond patterns are conserved between the two PSII (Fig. 1b and c). The only remarkable difference is observed at the slightly longer distances between **M** and the ligand water molecules in Sr^{2+} -PSII than in Ca^{2+} -PSII, 2.42–2.44 Å for Ca^{2+} and 2.55–2.56 Å for Sr^{2+} , predominantly due to the radii (Table 1).

The small radius of Mg^{2+} shortens the $Mg^{2+}\cdots W3$ and $Mg^{2+}\cdots W4$ distances (to 2.06 and 2.14 Å, respectively) (Table 1). The small radius of Mg^{2+} also breaks the H-bond between $W3\cdots W7$ (3.26 Å), which is energetically compensated for by the H-bond formation between $W3$ and D1-Glu189 (2.66 Å). Eventually, the alteration in the H-bond network occurs with respect to the Ca^{2+} - and Sr^{2+} -PSII (Fig. 1a), which may be associated with the inhibited O_2 -evolving activity in Mg^{2+} -PSII. In contrast, the large radius of Ba^{2+} increases the $Ba^{2+}\cdots W3$ and $Ba^{2+}\cdots W4$ distances significantly (to 2.68–2.70 Å, Table 1). However, the H-bond pattern of the H-bond network essentially remains unchanged with respect to the Ca^{2+} - and Sr^{2+} -PSII (Fig. 1d). The surface area of Ba^{2+} , which is 1.8 times larger than that of Ca^{2+} , may allow the third water molecule (W_{Ba}) to bind at Ba^{2+} in addition to $W3$ and $W4$

(Table 1). To evaluate the existence of the extra water molecule, W_{Ba} is placed at the resulting cavity near Ba^{2+} . QM/MM calculations show that W_{Ba} bridges the gap between D1-Glu189 and $W2$ via H-bonds (Fig. 1e). Thus, the alteration of the H-bond network is pronounced if the third water molecule is incorporated at the Ba^{2+} site. Note that no remarkable difference in the QM/MM-optimized geometry is observed when considering dispersion correction (Table S2, ESI†).

H-bond between TyrZ and D1-His190

The distance between Ca^{2+} and D1-Tyr161 (TyrZ) is 4.8 Å.¹ Ca^{2+} substitution induces deformations in the shape of a cluster of water molecules near TyrZ (*i.e.*, $W3$, $W5$, $W6$, and $W7$, Fig. 1), which are essential for forming the low-barrier H-bond between TyrZ and D1-His190.⁴³ Nevertheless, TyrZ···D1-His190 remains short (~ 2.5 Å, Fig. 1). The potential-energy profile for the H-bond indicates that TyrZ and D1-His190 form low-barrier H-bonds in all metal-substituted PSII (Fig. 2). It seems likely that the difference in the radius does not affect the formation of the low-barrier H-bond between TyrZ and D1-His190 if the H-bond network is maintained.

Energetics of the open- and closed- S_2 cubane conformations

In S_2 , the $Mn1(III)Mn2(IV)Mn3(IV)Mn4(IV)$ state adopts the open-cubane S_2 conformation, where the $Mn1(III)\cdots O5$ distance is larger than the $O5\cdots Mn4(IV)$ distance. In contrast, the $Mn1(IV)Mn2(IV)Mn3(IV)Mn4(III)$ state adopts the closed-cubane S_2 conformation, where the $Mn1(IV)\cdots O5$ distance is shorter than the $O5\cdots Mn4(III)$ distance.⁶⁸ In electron paramagnetic resonance (EPR) spectroscopy for the Mn_4CaO_5 cluster, the $g = 2$ multiline and $g > 4.1$ signals are observed (*e.g.*,⁶⁹). The $g > 4.1$ signals are classified into two cases: the $g = 4.1$ and $g = 4.8$ signals. Recent QM/MM calculations showed that the $g = 4.1$ signal corresponds to the closed-cubane conformation.⁷⁰ However, only the open-cubane S_2 conformation was identified in the XFEL structures, but not the closed-cubane S_2 conformation,^{71–73} probably because the open-cubane S_2 conformation is energetically more stable than the closed-cubane S_2 conformation.^{23,50,62,74} This also holds true for Mg^{2+} -PSII, Sr^{2+} -PSII, and Ba^{2+} -PSII: the differences in the alkaline-earth-metal and the H-bond network do not affect the stability of the open-cubane S_2 conformation with respect to the closed-cubane S_2 conformation (Fig. 3).

Discussion

Mn K-edge X-ray absorption spectroscopy²¹ and ENDOR²² studies suggested that the (electronic) structure of the Mn_4CaO_5 cluster remains essentially unaltered upon Ca^{2+} depletion. Consistently, the present QM/MM calculations show that Ca^{2+} -substitution/-depletion does not substantially affect the electronic structure of the Mn_4MO_5 cluster⁷⁵ (see also Table S3, ESI†).

The potential-energy profiles for the interconversion between the open- and closed-cubane S_2 conformations, namely, the energy



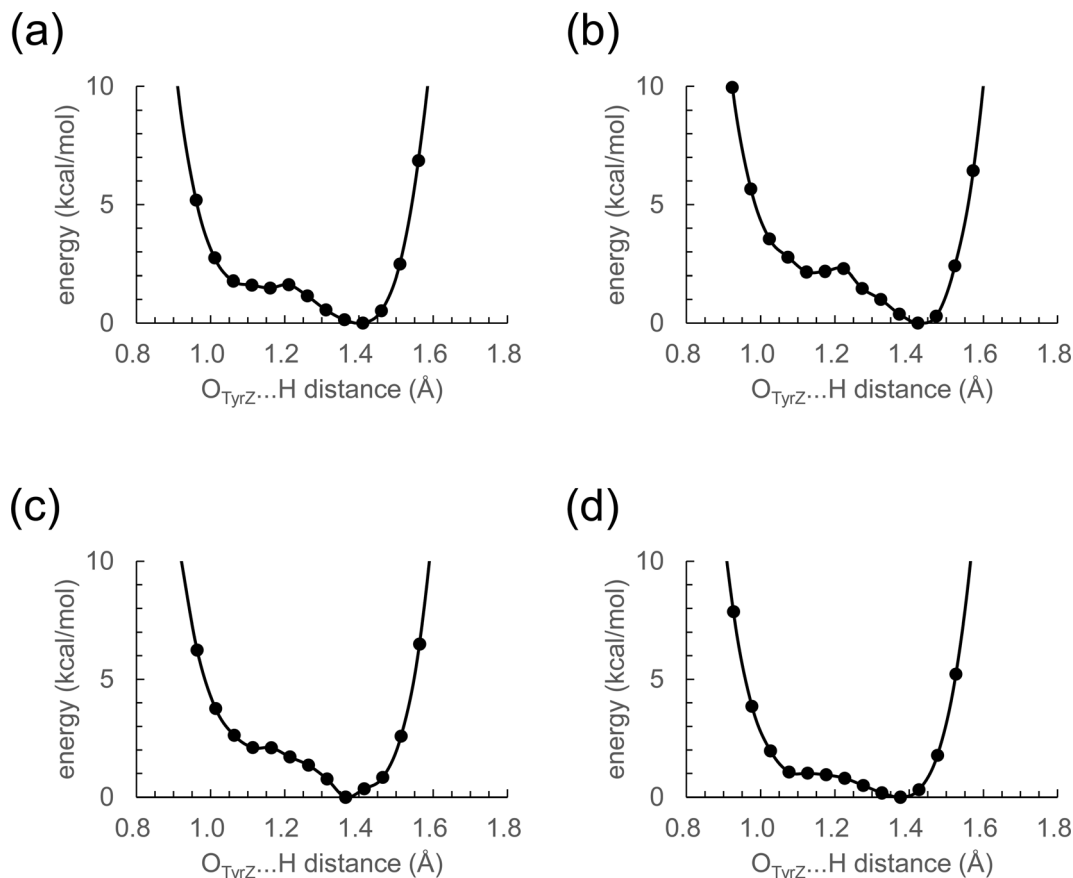


Fig. 2 Potential-energy profile of the H-bond between TyrZ and D1-His190 in S_2 . (a) Mg^{2+} -PSII. (b) Ca^{2+} -PSII. (c) Sr^{2+} -PSII. (d) Ba^{2+} -PSII.

difference between the open- and closed-cubane S_2 conformations, are similar in native Ca^{2+} -PSII and metal-substituted PSII (Fig. 3), which suggests that the inhibition of the interconversion of the two S_2 conformations is not responsible for the inhibition of O_2 evolution upon replacement of Ca^{2+} . Thus, the difference in the pK_a value for ligand-water deprotonation between alkaline earth metals may still be one of the plausible hypotheses for the inhibition mechanism.^{14,76,77}

The PSII crystal structure shows that Ca^{2+} has seven ligand groups (O1, O2, O5, D1-Asp170, D1-Ala344, W3, and W4).¹ In particular, O1, O2, and O5 form the Ca^{2+} binding site of the Mn_4CaO_5 cluster. Most distances with **M** increase as the radius of the alkaline earth metal increases (Fig. 4a). However, the $O5 \cdots M$ distance is exceptional. Intriguingly, the $O5 \cdots M$ distance in Ca^{2+} -PSII is the shortest among all metal-substituted PSII. Thus, Ca^{2+} is the alkaline earth metal that interacts most strongly with the Mn_4O_5 host region. The short $O5 \cdots Ca^{2+}$ distance, even shorter than the $O5 \cdots Mg^{2+}$ distance, suggests that Ca^{2+} may function most cooperatively with the Mn sites of the Mn_4O_5 cubane among all alkaline earth metals.

The $O5 \cdots M$ and $O2 \cdots M$ distances are identical (2.6 Å) only in Ca^{2+} -PSII, which suggests that the shape of the open-cubane Mn_3CaO_4 region is most symmetric with respect to the [**M** (Ca^{2+})-O1-O3-Mn3] plane among all metal-substituted PSII (Fig. 4b). The result presented here indicates that the binding

of Ca^{2+} is not the origin of the distorted cubane structure (e.g.,²⁰), but it minimizes the distortion of the cluster with respect to other alkaline earth metals, leading to the symmetric shape of the open-cubane Mn_3CaO_4 region. The minimized distortion with Ca^{2+} may indicate that the Mn_4CaO_5 cluster is most stable among all alkaline earth metal clusters. Thus, Ca^{2+} may contribute to the remarkably large turnover number of 10^5 for the Mn_4CaO_5 cluster in native PSII.⁷⁸

In summary, no significant difference is observed in the core structure or the characteristics of the H-bond between TyrZ and D1-His190 among the metal-substituted PSII (Fig. 2). This is consistent with the recent observations of synthetic Mn_4Ca clusters, in which Ca^{2+} can be structurally and energetically replaced by other metal ions (e.g., Y and Gd).⁷⁹

The characteristics of Sr^{2+} -PSII are closest to those of Ca^{2+} -PSII among Mg^{2+} , Sr^{2+} , and Ba^{2+} -PSII (Fig. 3). The H-bond pattern of the H-bond network of only Sr^{2+} -PSII is also consistent with that of Ca^{2+} -PSII (Fig. 1). The calculated pK_a value of a ligand water molecule at the Mn_4MO_5 cluster at the same level for Ca^{2+} and Sr^{2+} (~ 13) in the absence of the PSII protein environment (i.e., gas phase).⁷⁷ In contrast, the pK_a value for the ligand water molecule differs by 2 units between Mg^{2+} and Ba^{2+} ,⁷⁶ which largely originates from the difference in the radius. The difference in pK_a alters the H-bond distances with the ligand water molecules, whereas the difference in the



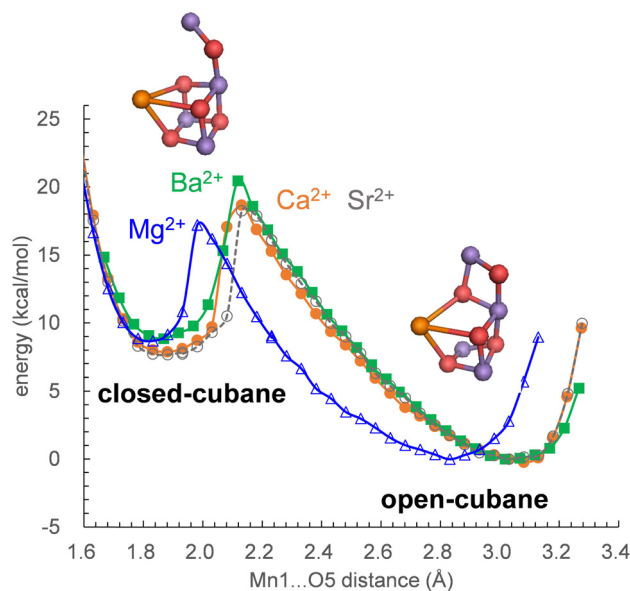
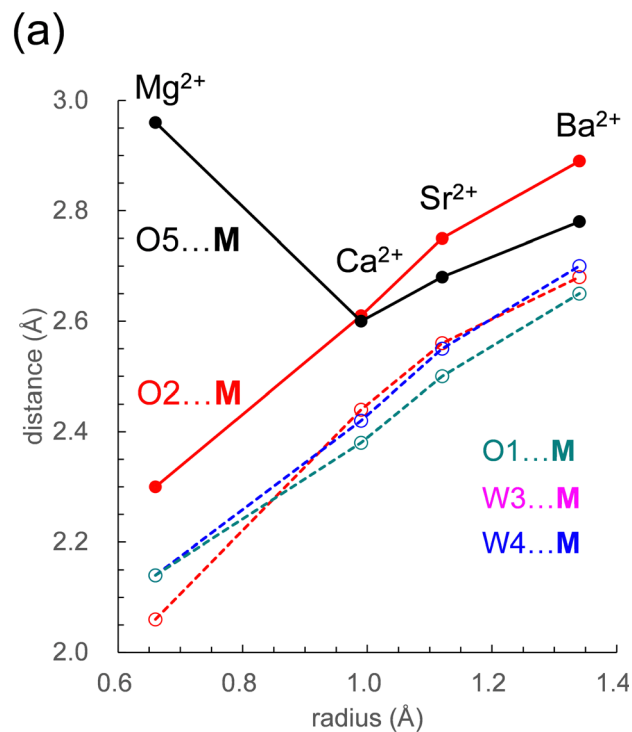


Fig. 3 Potential-energy profile for the O5 position along the Mn1...O5 and O5...Mn4 axes. The local energy minimum at the short Mn1...O5 distance (~ 1.8 Å) corresponds to the closed-cubane S_2 conformation, whereas the local energy minimum at the long Mn1...O5 distance (~ 3.0 Å) corresponds to the open-cubane S_2 conformation. The geometry was fully QM/MM-optimized at each point. Blue solid curve with open triangles: Mg^{2+} -PSII; orange solid curve with closed circles: Ca^{2+} -PSII; gray dotted curve with open circles: Sr^{2+} -PSII; green solid curve with closed squares: Ba^{2+} -PSII.

radius alters the distance between the metal center and the ligand water molecule. These differences are ultimately pronounced in the difference in the H-bond pattern of W3 in Mg^{2+} -PSII. In Mg^{2+} -PSII, W3 donates an H-bond to D1-Glu189, but the H-bond between W3 and W7 disappears, altering the H-bond network with respect to Ca^{2+} - and Sr^{2+} -PSIIs (Fig. 1a). In contrast, an increase in the radius compared to that of Ba^{2+} does not induce an alteration in the H-bond pattern of the H-bond network (Fig. 1d). Indeed, the difference in the pK_a value for the ligand water molecule among Ca^{2+} (12.8), Sr^{2+} (13.2), and Ba^{2+} (13.4) is very small,⁷⁶ which cannot explain the inactivity of Ba^{2+} -PSII. Only if a water molecule additionally binds at Ba^{2+} as the third ligand water molecule does it donate H-bonds to D1-Glu189 and W2, altering the H-bond network (Fig. 1e). According to recent X-ray free electron laser (XFEL) structures, a water molecule (O6) was inserted between W2 and D1-Glu189 during the S_2 to S_3 transition.^{72,73} However, in Mg^{2+} -PSII, W3 is closer to O5 and already donates an H-bond to D1-Glu189, which may inhibit O6 insertion (*i.e.*, the S_2 to S_3 transition). In Ba^{2+} -PSII, the binding site of the third ligand water molecule overlaps with the O6 binding site in the XFEL Ca^{2+} -PSII structure. Thus, Ba^{2+} with a third ligand water molecule may restrict the insertion of an extra water molecule (*e.g.*,^{71,72}) in the S_2 to S_3 transition. The low-barrier H-bond between TyrZ and D1-His190 remains unaffected even in the Mg^{2+} - and Ba^{2+} -PSIIs irrespective of the Ca^{2+} /metal binding site being relatively close to TyrZ (Fig. 2). Although Mg^{2+} and Ba^{2+} may not bind competitively with Ca^{2+} ,¹⁴ the observed alteration



(b)

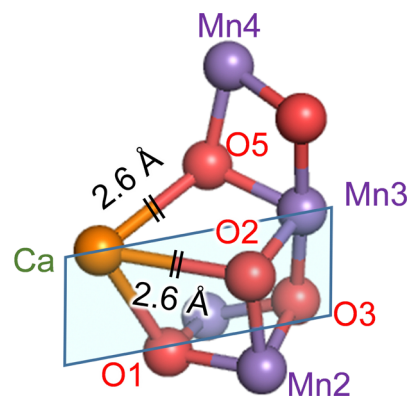


Fig. 4 (a) Dependence of the distances with **M** on the radius in the open-cubane S_2 conformation: O5...**M** (black solid line); W3...**M** (red dotted line); W4...**M** (blue dotted line); O1...**M** (green dotted line). (b) The open-cubane Mn_4CaO_5 structure and the [**M** (Ca^{2+})...O1...O3...Mn3] plane (sky blue square). See Table 1 for ionic radii.

in the “external” environment of the catalytic center (*e.g.*, ligand structure and H-bond network) may be associated with the inhibition mechanism for O_2 evolution if the metal-substituted PSIIs are properly assembled.

More importantly, Ca^{2+} exclusively minimizes the “internal” structure of the catalytic center. Ca^{2+} is the unique alkaline earth metal that (i) has the shortest O5...**M** distance (irrespective of the radius being larger than Mg^{2+}) and interacts most strongly with the Mn_4O_5 host region and (ii) equalizes the O5...**M** and O2...**M** distances (2.6 Å) and facilitates the formation of the symmetric cubane structure (Fig. 4a). The



resulting distortion-free Mn_4CaO_5 cluster is energetically advantageous with respect to the other metal-substituted clusters, which may contribute to the remarkably large turnover number of 10^5 in native PSII.⁷⁸ This may be one of the reasons why Ca^{2+} is the preferred redox-inactive site in nature as the catalytic O_2 -evolving center.

Conflicts of interest

There are no conflicts to declare.

Acknowledgements

We thank Keisuke Kawashima and Dr Toyokazu Ishida for useful discussion. This research was supported by JSPS KAKENHI (JP18H05155, JP18H01937, JP20H03217, and JP20H05090 to H. I. and 16H06560 and 18H01186 to K. S.), JST CREST (JPMJCR1656 to H. I.), and the Interdisciplinary Computational Science Program in CCS, University of Tsukuba. M. M. thanks Department of Biotechnology, Government of India for Ramalingaswami Re-entry Fellowship scheme (Ref. No. BT/RLF/Re-entry/41/2020, Dated: 15/12/2022) and S. N. Bose National Centre for Basic Sciences, Kolkata for computational facilities.

References

- 1 Y. Umena, K. Kawakami, J.-R. Shen and N. Kamiya, *Nature*, 2011, **473**, 55–60.
- 2 M. Suga, F. Akita, K. Hirata, G. Ueno, H. Murakami, Y. Nakajima, T. Shimizu, K. Yamashita, M. Yamamoto, H. Ago and J. R. Shen, *Nature*, 2015, **517**, 99–103.
- 3 S. E. J. Rigby, J. H. A. Nugent and P. J. O'Malley, *Biochemistry*, 1994, **33**, 10043–10050.
- 4 B. A. Diner, E. Schlodder, P. J. Nixon, W. J. Coleman, F. Rappaport, J. Lavergne, W. F. J. Vermaas and D. A. Chisholm, *Biochemistry*, 2001, **40**, 9265–9281.
- 5 T. Okubo, T. Tomo, M. Sugiura and T. Noguchi, *Biochemistry*, 2007, **46**, 4390–4397.
- 6 M. Mandal, K. Kawashima, K. Saito and H. Ishikita, *J. Phys. Chem. Lett.*, 2020, **11**, 249–255.
- 7 S. Vasil'ev, P. Orth, A. Zouni, T. G. Owens and D. Bruce, *Proc. Natl. Acad. Sci. U. S. A.*, 2001, **98**, 8602–8607.
- 8 S. Vasil'ev and D. Bruce, *Biophys. J.*, 2006, **90**, 3062–3073.
- 9 E. Schlodder and H. T. Witt, *J. Biol. Chem.*, 1999, **274**, 30387–30392.
- 10 H. Suzuki, M. Sugiura and T. Noguchi, *Biochemistry*, 2005, **44**, 1708–1718.
- 11 J. R. Shen, *Annu. Rev. Plant Biol.*, 2015, **66**, 23–48.
- 12 D. J. Vinyard and G. W. Brudvig, *Annu. Rev. Phys. Chem.*, 2017, **68**, 101–116.
- 13 A. Boussac and A. W. Rutherford, *Biochemistry*, 1988, **27**, 3476–3483.
- 14 J. S. Vrettos, D. A. Stone and G. W. Brudvig, *Biochemistry*, 2001, **40**, 7937–7945.
- 15 A. Boussac, F. Rappaport, P. Carrier, J. M. Verbavatz, R. Gobin, D. Kirilovsky, A. W. Rutherford and M. Sugiura, *J. Biol. Chem.*, 2004, **279**, 22809–22819.
- 16 C. F. Yocum, *Coord. Chem. Rev.*, 2008, **252**, 296–305.
- 17 V. K. Yachandra and J. Yano, *J. Photochem. Photobiol., B*, 2011, **104**, 51–59.
- 18 T. Ono, A. Rompel, H. Mino and N. Chiba, *Biophys. J.*, 2001, **81**, 1831–1840.
- 19 C.-I. Lee, K. V. Lakshmi and G. W. Brudvig, *Biochemistry*, 2007, **46**, 3211–3223.
- 20 K. Kawakami, Y. Umena, N. Kamiya and J.-R. Shen, *J. Photochem. Photobiol., B*, 2011, **104**, 9–18.
- 21 M. J. Latimer, V. J. DeRose, V. K. Yachandra, K. Sauer and M. P. Klein, *J. Phys. Chem. B*, 1998, **102**, 8257–8265.
- 22 T. Lohmiller, N. Cox, J. H. Su, J. Messinger and W. Lubitz, *J. Biol. Chem.*, 2012, **287**, 24721–24733.
- 23 K. Saito and H. Ishikita, *Biochim. Biophys. Acta*, 2014, **1837**, 159–166.
- 24 T.-A. Ono and Y. Inoue, *FEBS Lett.*, 1988, **227**, 147–152.
- 25 M. Sivaraja, J. Tso and G. C. Dismukes, *Biochemistry*, 1989, **28**, 9459–9464.
- 26 A. Boussac, J.-L. Zimmermann and A. W. Rutherford, *Biochemistry*, 1989, **28**, 8984–8989.
- 27 K. Saito, M. Mandal and H. Ishikita, *Biochemistry*, 2020, **59**, 3216–3224.
- 28 F. H. Koua, Y. Umena, K. Kawakami and J. R. Shen, *Proc. Natl. Acad. Sci. U. S. A.*, 2013, **110**, 3889–3894.
- 29 L. Vogt, M. Z. Ertem, R. Pal, G. W. Brudvig and V. S. Batista, *Biochemistry*, 2015, **54**, 820–825.
- 30 E. Y. Tsui, R. Tran, J. Yano and T. Agapie, *Nat. Chem.*, 2013, **5**, 293–299.
- 31 P.-H. Lin, M. K. Takase and T. Agapie, *Inorg. Chem.*, 2015, **54**, 59–64.
- 32 K. Saito, M. Nakagawa, M. Mandal and H. Ishikita, *Photosynth. Res.*, 2021, **148**, 153–159.
- 33 Y. Kimura, K. Hasegawa and T.-A. Ono, *Biochemistry*, 2002, **41**, 5844–5853.
- 34 H. Suzuki, Y. Taguchi, M. Sugiura, A. Boussac and T. Noguchi, *Biochemistry*, 2006, **45**, 13454–13464.
- 35 M. A. Strickler, L. M. Walker, W. Hillier and R. J. Debus, *Biochemistry*, 2005, **44**, 8571–8577.
- 36 T.-a Ono and Y. Inoue, *Biochim. Biophys. Acta*, 1990, **1020**, 269–277.
- 37 Z. Guo and B. A. Barry, *J. Phys. Chem. B*, 2017, **121**, 3987–3996.
- 38 Z. Guo, J. He and B. A. Barry, *Proc. Natl. Acad. Sci. U. S. A.*, 2018, **115**, 5658–5663.
- 39 R. J. Debus, *Biochemistry*, 2014, **53**, 2941–2955.
- 40 H. Kuroda, K. Kawashima, K. Ueda, T. Ikeda, K. Saito, R. Ninomiya, C. Hida, Y. Takahashi and H. Ishikita, *Biochim. Biophys. Acta*, 2021, **1862**, 148329.
- 41 K. Kawashima, T. Takaoka, H. Kimura, K. Saito and H. Ishikita, *Nat. Commun.*, 2018, **9**, 1247.
- 42 K. Saito, M. Nakagawa and H. Ishikita, *Commun. Chem.*, 2020, **3**, 89.
- 43 K. Saito, J.-R. Shen, T. Ishida and H. Ishikita, *Biochemistry*, 2011, **50**, 9836–9844.



- 44 A. A. Stuchebrukhov, *Phys. Rev. E*, 2009, **79**, 031927.
- 45 K. Saito, A. W. Rutherford and H. Ishikita, *Nat. Commun.*, 2015, **6**, 8488.
- 46 N. Sakashita, H. C. Watanabe, T. Ikeda, K. Saito and H. Ishikita, *Biochemistry*, 2017, **56**, 3049–3057.
- 47 B. R. Brooks, R. E. Bruccoleri, B. D. Olafson, D. J. States, S. Swaminathan and M. Karplus, *J. Comput. Chem.*, 1983, **4**, 187–217.
- 48 S. Nakamura and T. Noguchi, *J. Am. Chem. Soc.*, 2017, **139**, 9364–9375.
- 49 A. D. MacKerell, Jr., D. Bashford, R. L. Bellott, R. L. Dunbrack, Jr., J. D. Evanseck, M. J. Field, S. Fischer, J. Gao, H. Guo, S. Ha, D. Joseph-McCarthy, L. Kuchnir, K. Kuczera, F. T. K. Lau, C. Mattos, S. Michnick, T. Ngo, D. T. Nguyen, B. Prodhom, W. E. Reiher, III, B. Roux, M. Schlenkrich, J. C. Smith, R. Stote, J. Straub, M. Watanabe, J. Wiorkiewicz-Kuczera, D. Yin and M. Karplus, *J. Phys. Chem. B*, 1998, **102**, 3586–3616.
- 50 M. Amin, R. Pokhrel, G. W. Brudvig, A. Badawi and S. S. Obayya, *J. Phys. Chem. B*, 2016, **120**, 4243–4248.
- 51 M. Askerka, J. Wang, D. J. Vinyard, G. W. Brudvig and V. S. Batista, *Biochemistry*, 2016, **55**, 981–984.
- 52 M. Capone, D. Narzi and L. Guidoni, *Biochemistry*, 2021, **60**, 2341–2348.
- 53 S. Petrie, R. Terrett, R. Stranger and R. J. Pace, *Chem. Phys. Chem.*, 2020, **21**, 785–801.
- 54 P. E. Siegbahn, *Biochim. Biophys. Acta*, 2013, **1827**, 1003–1019.
- 55 M. Shoji, H. Isobe, J.-R. Shen, M. Suga, F. Akita, K. Miyagawa, Y. Shigeta and K. Yamaguchi, *Chem. Phys. Lett.*, 2019, **730**, 416–425.
- 56 M. Mandal, K. Saito and H. Ishikita, *J. Phys. Soc. Jpn.*, 2022, **91**, 091012.
- 57 P. J. Hay and W. R. Wadt, *J. Chem. Phys.*, 1985, **82**, 299–310.
- 58 QSite, 2012, version 5.8, Schrödinger, LLC, New York, NY.
- 59 K. Saito, T. Ishida, M. Sugiura, K. Kawakami, Y. Umena, N. Kamiya, J.-R. Shen and H. Ishikita, *J. Am. Chem. Soc.*, 2011, **133**, 14379–14388.
- 60 J. L. Zimmermann and A. W. Rutherford, *Biochemistry*, 1986, **25**, 4609–4615.
- 61 W. Ames, D. A. Pantazis, V. Krewald, N. Cox, J. Messinger, W. Lubitz and F. Neese, *J. Am. Chem. Soc.*, 2011, **133**, 19743–19757.
- 62 H. Isobe, M. Shoji, S. Yamanaka, Y. Umena, K. Kawakami, N. Kamiya, J. R. Shen and K. Yamaguchi, *Dalton Trans.*, 2012, **41**, 13727–13740.
- 63 K. Saito and H. Ishikita, *Biochim. Biophys. Acta*, 2019, **1860**, 148059.
- 64 G. Vacek, J. K. Perry and J. M. Langlois, *Chem. Phys. Lett.*, 1999, **310**, 189–194.
- 65 T. Takaoka, N. Sakashita, K. Saito and H. Ishikita, *J. Phys. Chem. Lett.*, 2016, **7**, 1925–1932.
- 66 K. Kawashima, K. Saito and H. Ishikita, *Biochemistry*, 2018, **57**, 4997–5004.
- 67 R. C. Weast, *CRC Handbook of Chemistry and Physics*, CRC Press, West Palm Beach, FL, 1978.
- 68 D. A. Pantazis, W. Ames, N. Cox, W. Lubitz and F. Neese, *Angew. Chem., Int. Ed.*, 2012, **51**, 9935–9940.
- 69 A. W. Rutherford, *Biochim. Biophys. Acta*, 1985, **807**, 189–201.
- 70 K. Saito, H. Mino, S. Nishio and H. Ishikita, *PNAS Nexus*, 2022, **1**, pgac221.
- 71 M. Suga, F. Akita, M. Sugahara, M. Kubo, Y. Nakajima, T. Nakane, K. Yamashita, Y. Umena, M. Nakabayashi, T. Yamane, T. Nakano, M. Suzuki, T. Masuda, S. Inoue, T. Kimura, T. Nomura, S. Yonekura, L. J. Yu, T. Sakamoto, T. Motomura, J. H. Chen, Y. Kato, T. Noguchi, K. Tono, Y. Joti, T. Kameshima, T. Hatsui, E. Nango, R. Tanaka, H. Naitow, Y. Matsuura, A. Yamashita, M. Yamamoto, O. Nureki, M. Yabashi, T. Ishikawa, S. Iwata and J. R. Shen, *Nature*, 2017, **543**, 131–135.
- 72 J. Kern, R. Chatterjee, I. D. Young, F. D. Fuller, L. Lassalle, M. Ibrahim, S. Gul, T. Fransson, A. S. Brewster, R. Alonso-Mori, R. Hussein, M. Zhang, L. Douthit, C. de Lichtenberg, M. H. Cheah, D. Shevela, J. Wersig, I. Seuffert, D. Sokaras, E. Pastor, C. Weninger, T. Kroll, R. G. Sierra, P. Aller, A. Butryn, A. M. Orville, M. Liang, A. Batyuk, J. E. Koglin, S. Carbajo, S. Boutet, N. W. Moriarty, J. M. Holton, H. Dobbek, P. D. Adams, U. Bergmann, N. K. Sauter, A. Zouni, J. Messinger, J. Yano and V. K. Yachandra, *Nature*, 2018, **563**, 421–425.
- 73 M. Suga, F. Akita, K. Yamashita, Y. Nakajima, G. Ueno, H. Li, T. Yamane, K. Hirata, Y. Umena, S. Yonekura, L. J. Yu, H. Murakami, T. Nomura, T. Kimura, M. Kubo, S. Baba, T. Kumasaka, K. Tono, M. Yabashi, H. Isobe, K. Yamaguchi, M. Yamamoto, H. Ago and J. R. Shen, *Science*, 2019, **366**, 334–338.
- 74 J. Yang, M. Hatakeyama, K. Ogata, S. Nakamura and C. Li, *J. Phys. Chem. B*, 2014, **118**, 14215–14222.
- 75 K. Saito, M. Mandal and H. Ishikita, *Biochemistry*, 2020, **59**, 3216–3224.
- 76 G. W. Brudvig, *Phil. Trans. R. Soc. Lond. B*, 2008, **363**, 1211–1219.
- 77 F. Pitari, D. Bovi, D. Narzi and L. Guidoni, *Biochemistry*, 2015, **54**, 5959–5968.
- 78 M. M. Najafpour, G. Renger, M. Holyńska, A. N. Moghaddam, E.-M. Aro, R. Carpentier, H. Nishihara, J. J. Eaton-Rye, J.-R. Shen and S. I. Allakhverdiev, *Chem. Rev.*, 2016, **116**, 2886–2936.
- 79 R. Yao, Y. Li, Y. Chen, B. Xu, C. Chen and C. Zhang, *J. Am. Chem. Soc.*, 2021, **143**, 17360–17365.

